Politecnico di Torino
Université Paris Cité

Master Thesis in Nanotechnoligies for ICTs and Quantum Devices

Politecnico di Torino

Université de Paris

Centre DE Nanosciences & DE Nanotechnologies

Quantum optics on a thin film lithium niobate on insulator platform

Centre de Nanoscience et Nanotechnologies

Supervisor:
Dr. Kamel Bencheikh

Candidate:
Enrico Maria Valentini

Academic year 2023-24

Contents

List of Figures

Acknowledgments

I would like to express my deep gratitude to my supervisor Dr. Kamel Bencheikh for all he has taught me during these months and for giving me the chance of finally approaching to the experimental work.

Alongside with him I want to also thank all my colleagues in the TONIQ group for helping me integrate as part of the team and for all the fruitful discussions.

I want also to thank my girlfriend and all my Politecnico colleagues in Torino and my NANOQUAD colleagues in Paris for all the moments and the help they gave me in every moment of these two years both in Italy and in France.

Finally I want to thank my family and friends from home, my parents in particular for always being there to support and advise me both in the bad and in the happy moments.

Summary

This report describes the objectives and the results of the internship project named "Quantum optics on a thin film lithium niobate on insulator platform" that I carried out in the TONIQ group at the Centre de Nanoscience et Nanotechnologies (C2N) under the supervision of Dr. Kamel Bencheikh.
This project was focused on the building of an optical setup devoted to explore a periodically poled lithium niobate waveguide and to characterize its properties in the realization of both classical and quantum optics results such as the realization of a single pass Optical Parametric Amplifier and the generation of squeezed states.
The structure of this report starts with an overview over the used device structure and materials, a glimpse at the theory that stands behind the involved processes and the presentation of the obtained results alongside with the challenges that arose in the process.

1 Introduction

1.1 Quantum optics

The description of optical phenomena has always been a wild and wide field of research in physics throughout the centuries, and it developed to a large extent even before the moment when the world witnessed the birth of quantum mechanics. Before that, the classical theory of electromagnetism was perfectly able to describe most of the linear and non-linear processes that occur in optics, but it was quite clear, from the very first experiments, that many phenomena originated from a more complex and unknown behaviour of light.[1]
Quantum optics is therefore a subject at the boundary between optics and quantum mechanics, focusing on the fundamental nature of light.
Like most phenomena in quantum mechanics, the quantum-optical ones only reveal themselves on closer inspection, so when technology allowed physicists to study the behaviour of light at extremely low intensities, ideally at the level of single photons, quantum optics was born, shifting the focus from the analysis of light to the measurement of its fluctuations.
This closer look was only possible thanks to the work of many pioneers in the field, such as R. Hanbury-Brown and R. Q. Twiss, who studied the correlations in the fluctuations of the photocurrents coming from two devices shone with the same light, or Chung Ki Hong, Zheyu Ou and Leonard Mandel, who investigated the concept of the indistinguishability of photons.
Once it was clear that the nature of light had more to offer, physicists and engineers raced to develop ever more sophisticated devices that could act as refined sources of single photons and detectors, and setups that could better analyse the light states generated; these advances paved the way for the discovery of new and even more mysterious phenomena, such as entanglement and quantum teleportation, which today form the basis of new systems of communication and computation entirely based on these concepts and capable of results unavailable with classical technology.

1.2 Periodically Poled Lithium Niobate

Unusual states of light are usually generated by non-linear interaction which indeed occur in particular crystals, the one in question is $LiNbO_3$ or lithium niobate (LN), an interesting material which shows several interesting properties in the optical domain which make it particularly suited for both classical and quantum optics application. Among such properties it is worth mentioning optical non linearity, which is fundamental in the framework of this report, Pockels effect , which makes it very useful for the realization of electro-optic modulators (EOM) and it can be integrated with materials like SiN which make LN based technology to be CMOS compatible[2]. The device analyzed during this internship is indeed made by thirty periodically poled lithium niobate (PPLN) waveguides, its complete structure will be detailed in section 3.1.

The fabrication of the PPLN waveguide analyzed in this project was carried out at the Royal Melbourne Institute of Technology (RMIT) and is described by the following steps:

- A $LiNbO_3$ wafer is implanted with a high dose of He^+ ions that form an implantation

layer where the crystal is significantly damaged, this is the ion slicing technique.

- The damaged wafer is thermally bonded to an insulating layer, usually made of SiO_2, after that the crackings are exploited to separate the bulk of the LN so to obtain a lithium niobate on insulator structure (LNOI).
- An optical load material, SiN in this case, is deposited on the LNOI by means of plasma enhanced chemical vapour deposition (PECVD).
- The optical load is lithographically patterned and etched by means of reactive ion etching (RIE) and finally the mask itself is removed.

The final waveguide structure, therefore, exhibits a layer of insulating material (SiO_2) covered by a thin film of lithium niobate (TFLN) and a final ridge of SiN below which the mode will be actually confined. The presence of this optical mode material provides both a tighter confinement, which lowers the optical losses with respect to standard wire waveguides (Ti indiffused or proton exchange ones), and as stated before, allows for better integration of this device with Si-based technology. Finally, it is worth pointing out that a SiN ridge waveguide also allows to overcome the issues present in the direct etching of $LiNbO_3$ ultimately simplifying the whole fabrication process through much better-established techniques used in Si-based technologies.

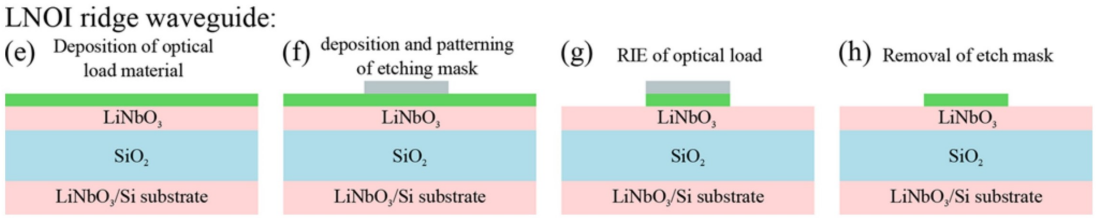

Figure 1: PPLN Fabrication
[3]

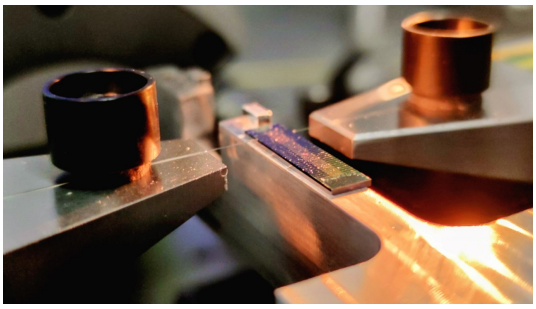

Figure 2: Periodically poled lithium niobate

The key step in the fabrication of a PPLN waveguide is the periodic poling technique which is realized by periodically patterning a series of electrodes connecting it to each waveguide, to such electrodes a high voltage (700V $\div$ 1000V) is applied, the result is to periodically flip the crystallographic axis of the waveguide. It is relevant to note that the actual position

of the electrodes on the guide depends on the crystallographic orientation of LN, the most common kinds are usually referred to as either "X-cut" or "Z-cut".

To understand the point of periodic poling it is possible to start by considering three waves propagating along z in a non-linear material with second order susceptibility tensor $\chi^{(2)}$, with frequencies ω_s, ω_i and ω_p; the evolution of such system is given by Poisson's equation as:

$$\begin{cases} \vec{\nabla}^2\vec{E_p} - \frac{1}{c^2}\frac{\partial^2}{\partial t^2}(\vec{E_p} + \frac{\vec{P_{NL}}}{\epsilon_0}) = 0 \\ E_p = E_{0p}(z)exp(ik_pz - \omega_p t) + c.c. \end{cases} \tag{1}$$

Where P_{NL} is the non-linear polarization, namely:

$$P_{NL}(z,t) = \epsilon_0\chi^{(2)}(E_s(z)exp(i(k_sz - \omega_s t)) + c.c.)(E_i(z)exp(i(k_iz - \omega_i t)) + c.c.) \tag{2}$$

which for simplicity can be rewritten considering only the term at $\omega_s + \omega_i$

$$P_{NL}(z,t) = \epsilon_0\chi^{(2)}E_s(t)E_i(t)exp(i(k_s + k_i)z) + c.c. \tag{3}$$

Therefore considering eq. 1 it becomes

$$i2k_p\frac{dE_p}{dz}exp(i(k_pz - \omega_p t)) + c.c. = \frac{1}{\epsilon_0 c^2}\frac{\partial^2}{\partial t^2}P_{NL} \tag{4}$$

$$\frac{dE_p}{dz}exp(ik_pz) = \frac{i\omega_p}{2\epsilon_0 n_p c}P_{NL}(z) \tag{5}$$

exploiting now 3

$$\frac{dE_p}{dz} = \frac{i\chi^{(2)}\omega_p}{2n_3 c}E_s(z)E_i(z)exp(i\Delta kz) \tag{6}$$

From which it is possible to derive, considering L the length of the crystal

$$|E_p(L)|^2 = (\frac{\chi^{(2)}\omega_p}{n_p c})^2|E_s|^2|E_i|^2\frac{L^2}{4}sinc^2(\frac{\Delta kL}{2}) \tag{7}$$

This quantity, the output field, is indeed maximized in the condition in which $\Delta k = k_s + k_i - k_p = 0$, which is known as the phase matching condition.
Such condition, which is of a crucial importance in exploiting non-linear optical processes, is usually achieved by exploiting the natural birefringence of many non-linear crystals. Whenever this is not the case is however possible to address a similar condition, which is the one realized by periodic poling indeed, the quasi phase matching condition (QPM), namely:

$$k_p = k_s + k_i + \frac{2\pi}{\Lambda} \tag{8}$$

where Λ is the period of the poling and k_p, k_s and k_i are the wavevectors of the pump, signal and idler waves, QPM is necessary to achieve a net flow of energy across the sample which

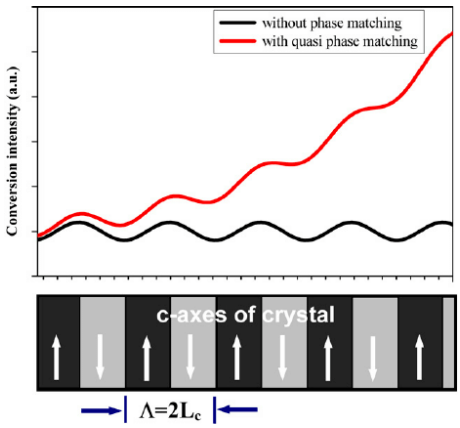

Figure 3: Quasi-Phase Matching Condition

allows the second harmonic generation or spontaneous parametric down-conversion processes for example; as it can be seen from the plot in figure 3, QPM condition allows to obtain an increasing conversion intensity along the length of the crystal [4].
It is worth observing that lithium niobate is also birefringent, that being said, LN natural birefringence, which addresses the $d_{31} = 4.35pm/V$ coefficient of the non-linear tensor cannot be exploited in a waveguide but only in a bulk system, QPM, on the other hand, addresses the coefficient $d_{33} = 27pm/V$ which is compatible to the waveguide structure and provides a good efficiency as well. [5].

2 Objectives

The objective of this internship is to use a periodically poled lithium niobate (PPLN) platform as the one previously described for the generation of squeezed states, a peculiar kind of non-classical light states which can only be generated by exploiting a non-linear medium such as $LiNbO_3$. In this section the essential theoretical background on squeezed states, their generation and detection, will be covered.

2.1 Squeezed States

As stated in the introduction, to understand the concept of squeezing of light states, the focus must be shifted towards the fluctuations of the field, more precisely to its uncertainties.
First, it is possible to define a minimal uncertainty state as a light state with a minimal uncertainty relation, namely, using Heisenberg uncertainty principle:

$$\Delta\hat{X_1}\Delta\hat{X_2} \geq \frac{1}{4} \tag{9}$$

Where ΔX_1 and ΔX_2 are the uncertainties over the quadratures of the field, which can be defined in terms of position and momentum operators in the phase dependent field quadrature [6]:

$$\hat{X}(\theta) = \hat{x}cos(\theta) + \hat{p}sin(\theta) = \frac{1}{\sqrt{2}}(\hat{a}^\dagger e^{i\theta} + \hat{a}e^{-i\theta}) \tag{10}$$

Choosing any couple of orthogonal quadratures X_1 and X_2 are obtained, namely

$$\begin{cases} \hat{X}_1 = \frac{1}{\sqrt{2}}(\hat{a}^\dagger + \hat{a}) \\ \hat{X}_2 = \frac{i}{\sqrt{2}}(\hat{a}^\dagger - \hat{a}) \end{cases} \tag{11}$$

The case of minimal uncertainty is indeed the one of two particularly common cases, vacuum states and coherent states, which are defined respectively as [7]

$$\begin{cases} |0\rangle \\ |\alpha\rangle = e^{-\frac{1}{2}|\alpha|^2} \sum_{n=0}^{\infty} \frac{\alpha^n}{(n!)^{\frac{1}{2}}} |n\rangle \end{cases} \tag{12}$$

Where α is the amplitude of the coherent state and $|\alpha|^2$ is the mean photon number contained in the field.
A common way of representing such states is in phase-space by means of its quadratures, more specifically using Wigner function

$$W(x,p) = \frac{1}{2\pi} \int_{-\infty}^{+\infty} exp(ipx')\langle x - \frac{x'}{2}|\hat{\rho}|x + \frac{x'}{2}\rangle dx' \tag{13}$$

Where $\hat{\rho}$ is the density matrix of the state, Wigner function is represented graphically for the two considered kind of states in figure 4.

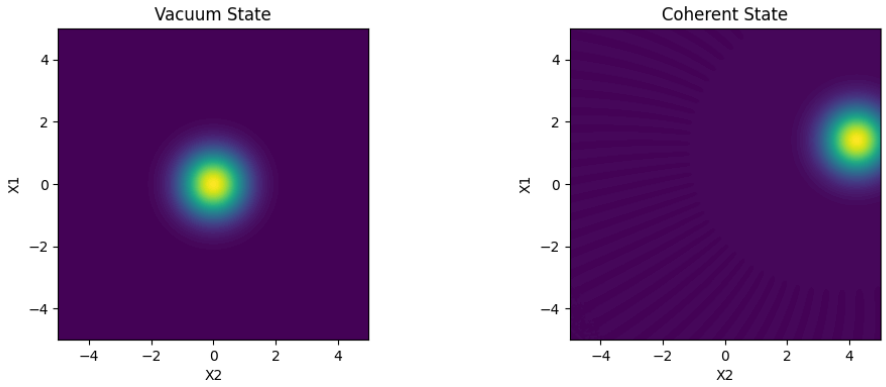

Figure 4: Vacuum States and Coherent States

Squeezed states are themselves minimal uncertainty states which can be obtained starting from either a vacuum state or a coherent state by applying the squeezing operator defined as

$$\begin{cases} \hat{S}(\xi) = exp(\frac{1}{2}\xi^* \hat{a}^2 + \frac{1}{2}\xi^* \hat{a}^{\dagger 2}) \\ \xi = r_s exp(i2\theta_s) \end{cases} \tag{14}$$

Where r_s is the squeezing parameter and θ_s is the squeezing angle. The resulting states plotted in terms of their Wigner function are represented in figure 5.

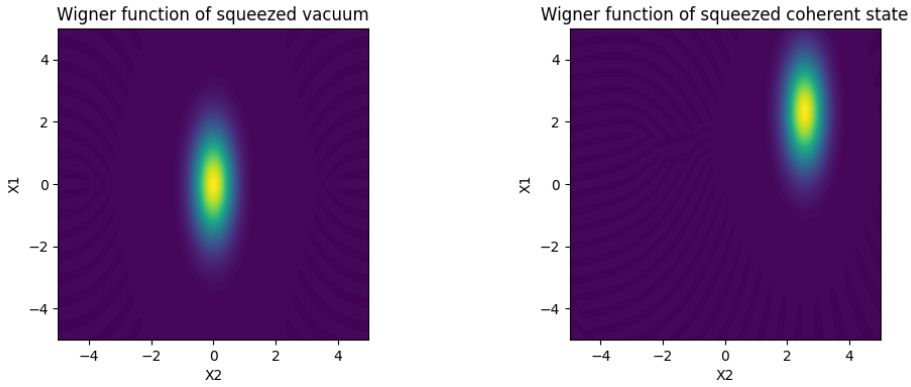

Figure 5: Minimal Uncertainty States

It is worth remarking that squeezed states are indeed minimal uncertainty states as much as vacuum and coherent states are themselves, the true feature that distinguishes them is the fact that the uncertainties in the two quadratures of the field are correlated to one another by the squeezing parameter. This means that it is possible to preserve the minimal uncertainty over the two quadratures by "squeezing" one and enlarging the other, thus, achieving an uncertainty over one quadrature which is lower than the standard quantum limit (SQL).

The squeezing is quantified though the measurement of the variance of the phase dependent

quadrature which, for a given couple of orthogonal angles gives the variances over the two individual quadratures, namely [1]

$$\begin{cases} V_1 = exp(2r_s) \\ V_2 = exp(-2r_s) \end{cases} \tag{15}$$

2.2 Generation of squeezed states

The generation of squeezed states of light can be achieved using a non-linear optical process, in this section the main and most used nowadays will be presented.

2.2.1 Four Wave Mixing (4WM)

The Four-wave mixing effect can be described as follows. We can consider three beams impinging on a non-linear medium, having a $\chi^{(3)}$ non-linear susceptibility tensor, with frequencies ν_p, $\nu_p - \Omega$ and $\nu_p + \Omega$; the result in this scheme is the amplification of the pump beam.[1]

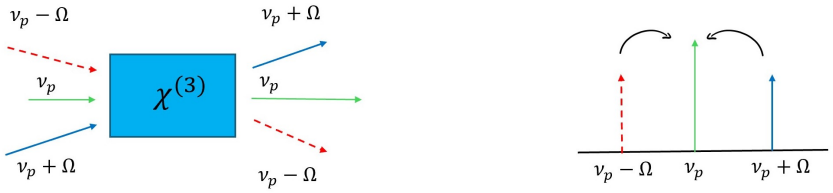

Figure 6: Four Wave Mixing process

The phenomenon with which 4WM generates squeezed states from a classical one is a selective amplification of the two quadratures, in a phasor diagram this can be represented as follows.

$$\begin{cases} \delta X1_{out}(t) = (1+C)\delta X1_{in}(t) \\ \delta X2_{out}(t) = (1-C)\delta X2_{in}(t) \end{cases} \tag{16}$$

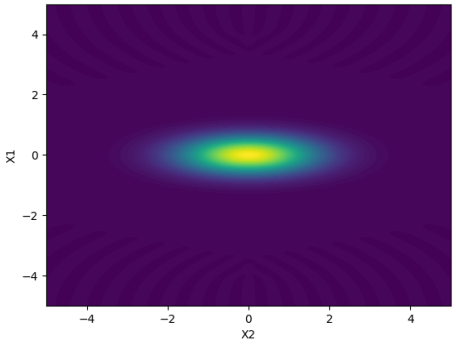

Figure 7: Wigner function for four wave mixing

2.2.2 Kerr Effect

Kerr effect is based on the dependence of the refractive index on the intensity of the light impinging on a $\chi^{(3)}$ medium, therefore intensity fluctuations will modulate the refractive index which consequently induces a modulation of the phase.[1] The net result is, therefore,

that amplitude modulation affects phase modulation, therefore, the two fluctuations in the output of the medium will be correlated with one another in the following way:

$$\begin{cases} \delta X1_{out}(t) = \delta X1_{in}(t) \\ \delta X2_{out}(t) = \delta X2_{in}(t) + \frac{4\pi n_0 n_2 L}{\lambda} X1^2 \delta X1_{in}(t) \end{cases} \tag{17}$$

Squeezing is therefore obtained by means of this coupling between the two quadratures which can be represented as:

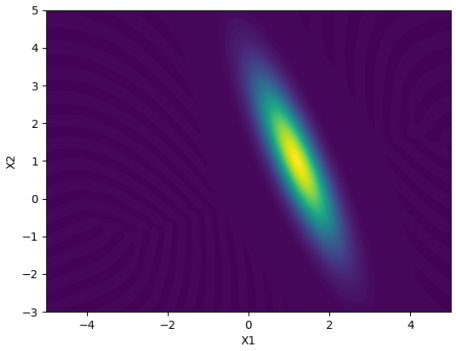

Figure 8: Wigner function for Kerr effect

2.2.3 Optical Parametric Interaction

In the optical parametric interaction, a pump and a signal beam impinge on the non-linear crystal, the pump (represented at $\omega_p = 780nm$ in figure 9) will be "down converted" generating another signal beam at frequency ω_s; the net result of this process is the amplification of the signal beam by the generation of a second one which phase is related to the pump beam as $\phi_p = 2\phi_s$.

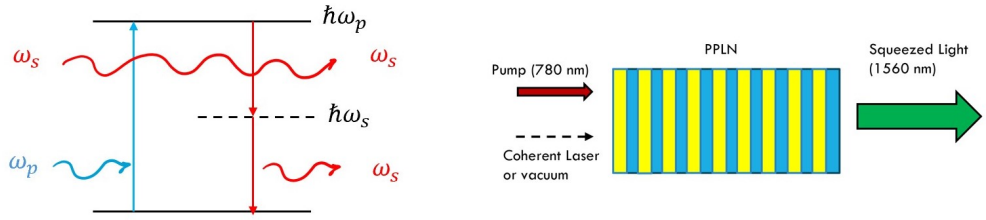

Figure 9: Scheme of an Optical Parametric Amplifier

As figure 9, shows two possibilities will be considered for the signal, if only the pump beam is impinging on the medium input the result will be the so called "squeezed vacuum" while if a coherent beam is applied as well the result will be known as "bright squeezed state". The hamiltonian that describes this process is the following[8]:

$$\begin{cases} \hat{H} = i\hbar\gamma(\hat{a}^2 - \hat{a}^{\dagger 2}) \\ \gamma \propto \chi^{(2)} E_p \end{cases} \tag{18}$$

It is worth pointing out both the second order dependence over the creation and annihilation operators and from the second order non-linearity coefficient $\chi^{(2)}$ which relates this process to the actual non-linear character of $LiNbO_3$; as a matter of fact the evolution of the system is regulated by the following equations:

$$\begin{cases} \frac{d\hat{a}}{dt} = -\gamma\hat{a}^\dagger \\ \frac{d\hat{a}^\dagger}{dt} = -\gamma\hat{a} \end{cases} \tag{19}$$

Using now the quadratures definition as in eq.11

$$\begin{cases} \hat{X}_1 = \frac{1}{\sqrt{2}}(\hat{a} + \hat{a}^\dagger) \\ \hat{X}_2 = \frac{i}{\sqrt{2}}(\hat{a}^\dagger - \hat{a}) \end{cases} \tag{20}$$

The equations 19 are rewritten in terms of quadratures as

$$\begin{cases} \frac{d\hat{X}1}{dt} = -\gamma\hat{X}_1 \\ \frac{d\hat{X}2}{dt} = \gamma\hat{X}_2 \end{cases} \tag{21}$$

The solution of such equations express the evolution of the two quadratures at the output of the medium as a function of the quadratures at the input

$$\begin{cases} \hat{X}1_{out} = exp(-\gamma\tau)\hat{X}_{1in} \\ \hat{X}2_{out} = exp(\gamma\tau)\hat{X}_{2in} \end{cases} \tag{22}$$

From these equations it becomes evident that the parametric amplification process indeed distinguishes the amplification between the two quadratures, amplifying one while de-amplifying the other, this property also extends to their respective fluctuations which indeed allows to generate squeezed states.[1]
In conclusion, the parametric amplification process is the one chosen for the generation of squeezed states in the work presented in this report, thanks to the high second-order non-linearity of lithium niobate addressed by the periodic poling technique. As stated above the aim is to realize an optical parametric amplifier (OPA) by pumping the PPLN waveguide at with a 780nm beam to obtain squeezed light at the frequency of 1560nm.

2.3 Detection of squeezed states

This last introductory section is devoted to the description of how it is possible to detect a squeezed state, meaning the measurement of the quadratures fluctuations.
The balanced homodyne detection is the most common method of detecting squeezed light, the setup needed for this approach is schematized in figure 10.

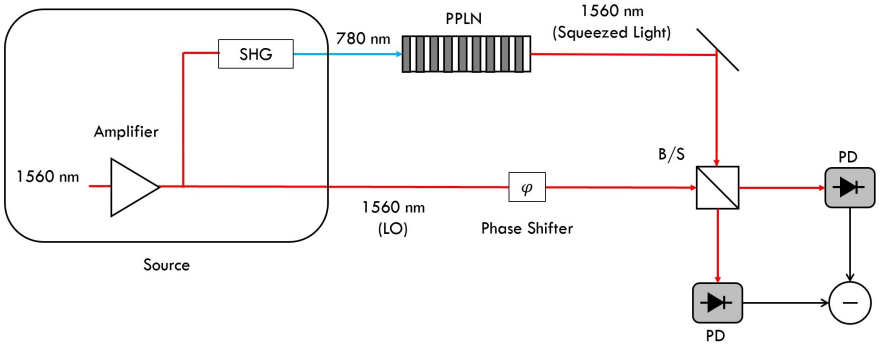

Figure 10: Homodyne detection setup

In a balanced homodyne detection scheme, the squeezed state is mixed, using a beam splitter, with a local oscillator field delivered by the same source delivering the pump exciting the PPLN. The light at the two output ports of the beam splitter will be fed to two photodiodes which photocurrents will be subtracted from one another ultimately leaving only the fluctuations of the field.[9]

Given that the field and the LO are described by the operators $\hat{a}$ and $\hat{a}_{LO}$, the output ports of the beam splitter will give [6]

$$\begin{cases} \hat{a}_1 = \frac{1}{\sqrt{2}}(\hat{a} + \hat{a}_{LO}) \\ \hat{a}_2 = \frac{1}{\sqrt{2}}(\hat{a} - \hat{a}_{LO}) \end{cases} \rightarrow \begin{cases} \hat{n}_1 = \hat{a}_1^\dagger \hat{a}_1 = \frac{1}{2}(\hat{a}^\dagger\hat{a} + \hat{a}^\dagger\hat{a}_{LO} + \hat{a}_{LO}^\dagger\hat{a} + \hat{a}_{LO}^\dagger\hat{a}_{LO}) \\ \hat{n}_2 = \hat{a}_2^\dagger \hat{a}_2 = \frac{1}{2}(\hat{a}^\dagger\hat{a} - \hat{a}^\dagger\hat{a}_{LO} - \hat{a}_{LO}^\dagger\hat{a} + \hat{a}_{LO}^\dagger\hat{a}_{LO}) \end{cases} \tag{23}$$

Considering the local oscillator as a classic field is is possible to replace the operators with their expectation values ($\alpha_{LO}e^{\pm i\theta_s}$), therefore, the difference in the number of photons at each port can be mathematically linked to the phase depended field quadrature as follows.

$$\begin{aligned} \hat{n}_2 - \hat{n}_1 &= \hat{a}^\dagger\hat{a}_{LO} + \hat{a}_{LO}^\dagger\hat{a} \\ &= \alpha(\hat{a}^\dagger e^{i\theta_s} + \hat{a}e^{-i\theta_s}) \\ &= \sqrt{2}|\alpha|\hat{X}_\theta \end{aligned} \tag{24}$$

3 Results

This section aims at explaining the results obtained in the four phases in which this internship workflow has been divided.

3.1 Waveguides SHG characterization

The device is the one represented in figure 2, it is composed by three section of ten waveguides each, all of them are characterized in the following way by the periodic poling:

- Each section has a constant poling period, respectively $4.87\mu m$, $4.93\mu m$ and $4.98\mu m$.
- Inside each section the first six waveguides are divided in three couples with a progressively increasing poling length, as shown in the last plot of figure 12b.
- the last four waveguides of each section have both the same poling period and length.

The first phase was necessarily the characterization of each waveguide present in the device, this has been done employing the Second-Harmonic-Generation (SHG) process, also known as frequency doubling, such frequency is the one targeted by QPM condition. It is worth pointing out that this characterization technique has been chosen being the opposite process concerning the one exploited in the parametric amplification one, the SPDC, therefore, the now doubled frequency will later serve itself as the pump of the OPA[10].
The experimental setup that was realized to perform the characterization was the one reported in figure 11

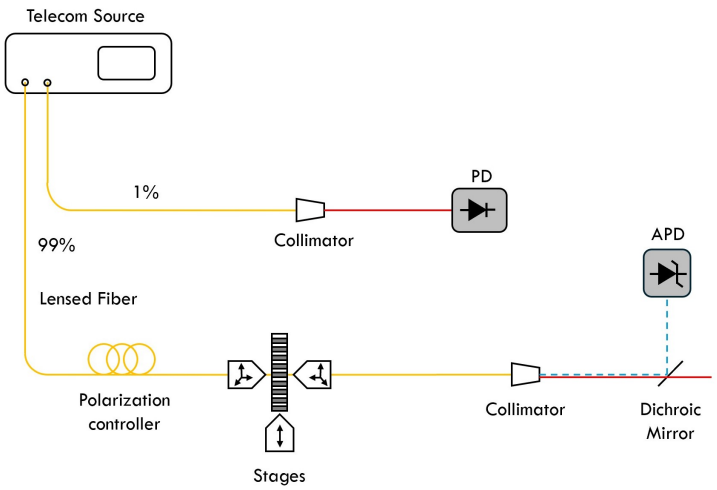

Figure 11: SHG characterization Setup

The source is a Tunics T100R laser able to emit wavelengths in the range 1490-1650 nm, to its channels, to improve the coupling, two lensed telecom fibers (OZ Optics) were exploited for the input and output coupling. Furthermore, a monitoring output only taking 1% of the total emitted power which was monitored by a Photo Diode (PD, New Focus 1811-FS) while the second one with 99% of the total power passed through a polarization controller

and ended in the device section, here three translation stages served to align the fiber tip to the actual waveguide portion of the device and to select among the different waveguides as well. Once out-coupled in the second, identical lensed fiber, the emitted SHG light goes into free space through a fiber collimator, here a dichroic mirror deflects it into an Avalanche Photo Diode (APD) removing the remaining pump; for the sake of completeness, it is worth saying that to improve the detection sensitivity, the intensity of the fundamental laser was modulated by driving its current with a sine-wave function at 35 kHz.

The measurement procedure was the following one:

- A visible laser was used to align the lensed fibers into the waveguide, probing the coupling between input and output.
- A wavelength sweep was performed to identify the characteristic wavelength of the waveguide.
- The SHG signal was maximized by fine tuning the alignment of the fibers and the polarization.
- A more resolved wavelength sweep was performed to acquire the complete spectrum.

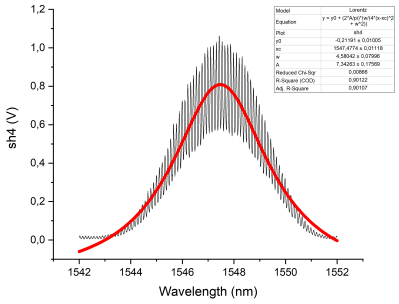

(a) SHG spectrum example

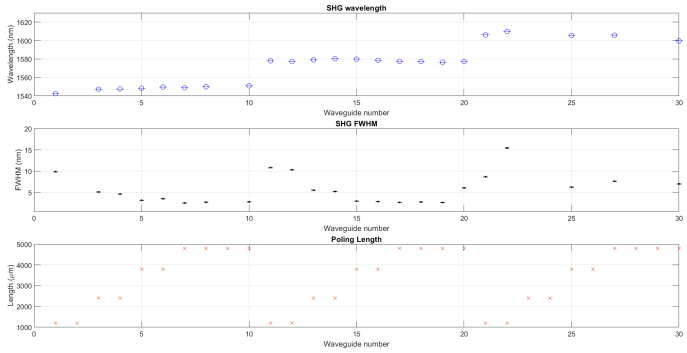

(b) SHG characterization results

As can be observed from the figure 12a, the thirty waveguides are divided into sections of ten sharing the same poling period, indeed both the SHG wavelength and the Full Width Half Maximum (FWHM) characterization reproduce this scheme. As the plot in figure 12b shows, the SHG wavelengths for the three section of waveguides were: $1548 \pm 2nm$ for $\Lambda = 4.87\mu m$, $1578 \pm 1nm$ for $\Lambda = 4.93\mu m$ and $1605 \pm 2nm$ for $\Lambda = 4.98\mu m$, It is also relevant underlying the absence of some data points due to particularly poor coupling conditions encountered in some of the waveguides, these may relate to defects or damages in the device due to the time elapsed from the fabrication.

3.2 Temperature characterization of QPM condition

The second stage of this internship project was to characterize the way in which the temperature affects the quasi-phase matching condition so to achieve the required wavelengths, to perform this analysis the device was positioned on a case made of copper which was designed to host a HT24S ceramic heater and PT100 temperature sensor, both these devices were controlled by a TEC300 temperature controller.
The increment or reduction of the temperature of the crystal yields a red-shift or blue-shift respectively in the wavelength targeted by QPM condition, in this experiment, heating rather than cooling was exploited to avoid condensation of the ambient water and photorefractive effect.

The analysis involved the progressive increase of the temperature of the device in steps of 5°C each from room temperature (25°C) up to 100°C, using the above described setup, and the characterization of a single, selected waveguide with the same procedure explained in the last section, by means of SHG.
For each temperature step, therefore, the SHG spectrum was acquired to identify the peak wavelength associated to it.

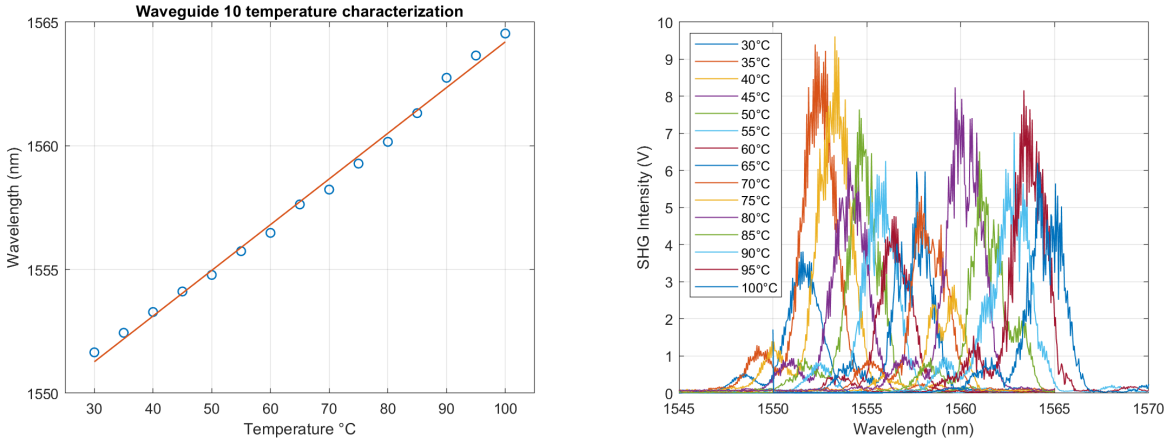

Figure 13: Temperature characterization of waveguide n.10

The first plot in figure 13 shows the peak values of the wavelength as a function of the temperature while the following shows the actual shift of the SHG spectrum as for the different considered temperatures, clearly both plot confirm the red-shifting yielded by temperature rise; the choice of a waveguide characterized by $\Lambda = 4.87\mu m$ and $L = 4800\mu m$, is motivated mostly by the need for heating, and therefore red-shifting, rather than cooling the device as stated before, according to the characterization results presented in figure 12b, placed the two other sections of waveguides out of reach for the 1560nm target wavelength needed for the project.
As the plot in figure 14 remarks, by heating up the temperature of waveguide n.10 up to 80°C, it was possible to shift its peak wavelength from 1550nm up to 1560nm, correctly matching the aimed value, a finer tuning of the temperature of course allows to modify in a

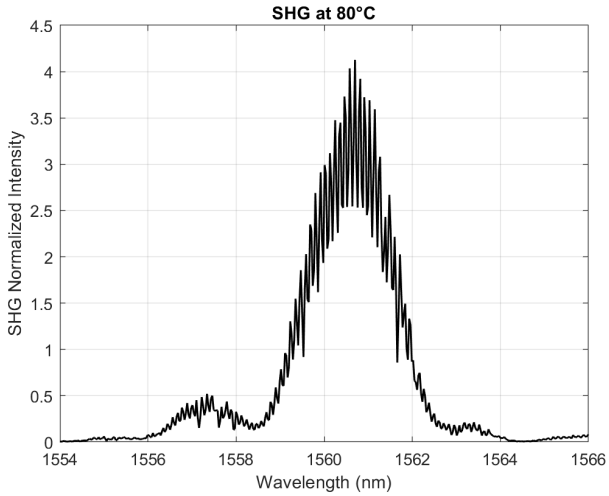

Figure 14: SHG spectrum at 80°C

more accurate way the red-shifting.
In the following sections a specific 780nm source (ELYSA780) will be used for both the pump and the signal beams, respectively at 780.3nm and 1560.48nm, therefore its temperature characterization was performed as well.

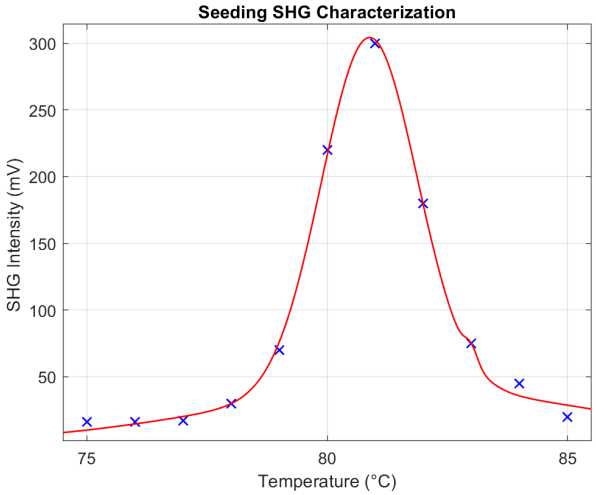

Figure 15: SHG spectrum vs.temperature

From figure 15, it can be seen that indeed the maximum of the SHG signal for the aforementioned 1560.48nm wavelength is generated in the interval between 80°C and 81°C, this experiment also allowed to better appreciate a limitation in the temperature stability of the device, which directly affected the SHG signal yielding non-negligible oscillations in it that also limited the achievable resolution for this characterization.

3.3 Optical parametric amplifier

The aim of this section is to analyze the classical result of an OPA process that is to say the phase-dependent amplification, this is realized by means of the setup shown in figure 16.

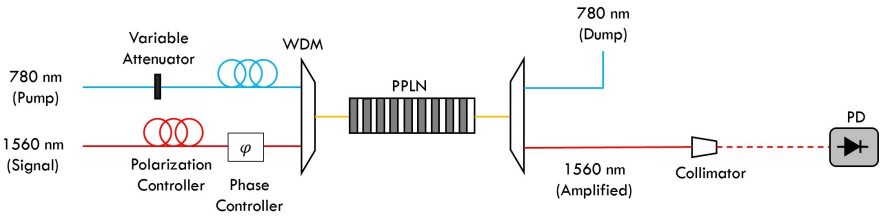

Figure 16: OPA Setup

The setup features two sources, one at 780nm (the pump) along which line a polarization controller and a variable attenuator to control the injected power are inserted, and one at 1560nm (the signal), along which line are present another polarization controller and the key point of this first stage which is a fibered phase controller which is driven by a 1Hz triangular wave to modify the phase of the signal beam. Both fibers are joint by a wavelength division multiplexer (WDM) which common port is itself connected to the lensed fibered used in the previous sections to improve the coupling, therefore, the PPLN waveguide is pumped at the same time by both beams. Similarly at the output another WDM is exploited to separate the two components, while the remaining pump contribution is dumped, the amplified signal is collected by a fiber collimator and detected using a photodiode.
The net result of this is the amplification of the signal beam as described by the process represented in figure 9, such amplification however, thanks to the phase variation introduced in the signal beam shows an oscillating behaviour, which oscillations are depending on the phase value, therefore obtaining a phase dependent amplification.

From the implementation of this setup however, several challenges arose that complicated the measuring of the phase dependent gain; the aforementioned temperature oscillations, alongside with phase noise revealed themselves to be too severe to allow for a clean observation of the intended phase oscillations, furthermore the seeding power provided by the pump source was also revealed to be too high, further complicating the measurements. To face all these challenges some changes had to be introduced in the setup configuration to limit these detrimental effects.
As figure 17 shows, the pump injection section features some added components, the idea behind this change was to exploit a two collimator configuration to go into free space to use a chopper as modulation source for the detector, using a lock-in amplifier, in order to highlight in the observed signal the phase oscillations over the noisy ones. Finally, to account for the high power of the seeding, the fiber connecting it was slightly dislodged from its connection with the aim of reducing the amount of power flowing into the seeding to some tenths of μW.

By implementing the above described changes into the setup it was possible to actually observe the phase dependent oscillations as shown in figure 18

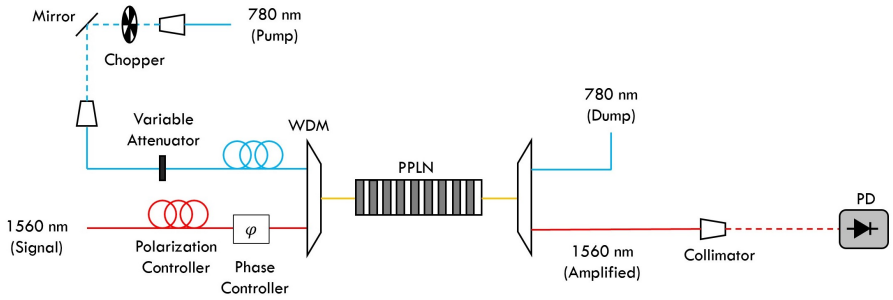

Figure 17: Modified OPA Setup

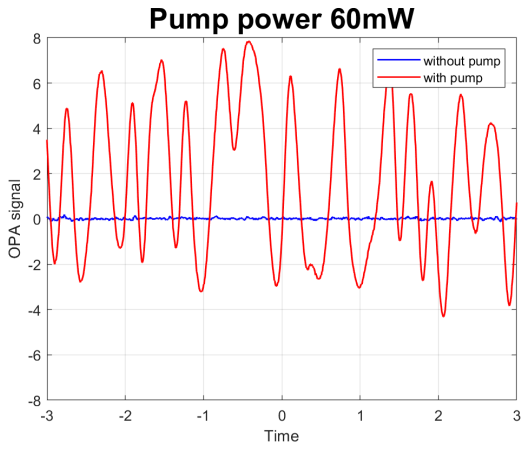

Figure 18: OPA phase-dependent Gain

As expected, when the pump is cut-off the gain is nullified; instead by adding it the gain starts to oscillate with the frequency defined by the function generator controlling the phase shifter, furthermore, by adjusting the relative power of the seeding and the pump itself it is possible to improve the quality of the signal and therefore, the gain. It is also worth pointing out that the obtained result is still plagued by both thermal and phase noise which could be effectively counteracted by insulating the device and the fibers.
It is also worth pointing out that by increasing the power of the pump is possible to increase the amplitude of the oscillations and therefore the amplification and de-amplification gain themselves as shown in figures 19.

3.4 Squeezing measurements

This section is devoted to describing the procedures relating the measurements of the squeezing using homodyne detection such as the characterization of the balanced homodyne detector, the noise level, the used experimental setup etc.

3.4.1 Balanced homodyne detector characterization

The characterization of the balanced homodyne detector (BHD), which internal structure is the same one reported in figure 10 was aimed at observing the response of the detector

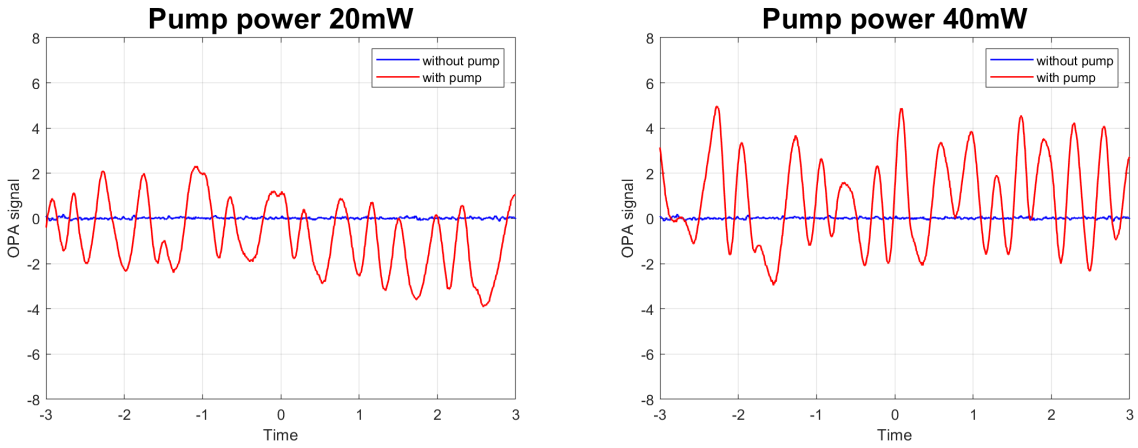

Figure 19: 20mW vs 40mW pump power

depending on the injected power, it exploited a rather simple setup as the one shown in figure 20.

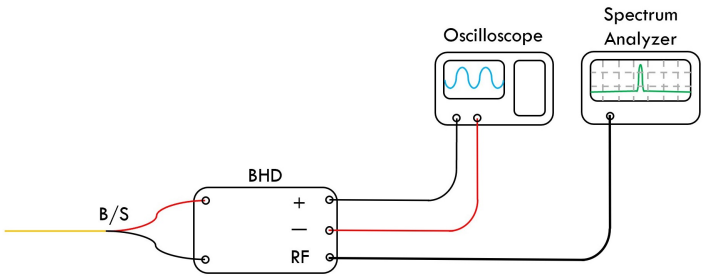

Figure 20: BHD Setup

In this setup, a fiber beam splitter is used to split the input beam, coming from the same source exploited in the SHG characterization stage (Tunics T100R), into the two input ports of the BHD which itself exhibits three outputs; the first two are monitoring outputs which are both collected and sent to a digital oscilloscope to measure the difference in their signal; a perfect balancing of both the detector and the beam splitter would yield a zero difference between the two channel certifying the correct balance.
The third (RF) output is connected to a spectrum analyzer which aim is to observe the actual differences in the fluctuations of the two signals, therefore, in presence of two coherent, identical beams, as it is supposed to be in this case, giving, ideally, the so called Quantum Noise Limit (QNL).

The characterization was exactly devoted to evaluate first the evolution of the QNL with respect to the power of the source. As figure 21 shows, a linear dependence of the noise level of the BHD is observed with respect to the power. For the sake of completeness, in the same figure the logarithmic plot showing the dBm values of the noise level is reported.

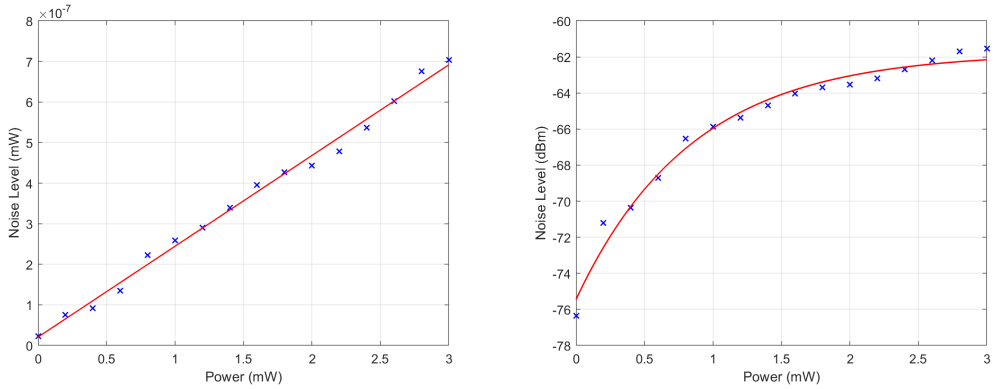

Figure 21: Noise level power dependence

To have a complete picture of the BHD characterization, a power sweep with the same source, which wavelength was fixed at 1560nm, was performed between 0.2mW and 2.5mW to observe up to which value the BHD is able to provide a proper response without saturating.

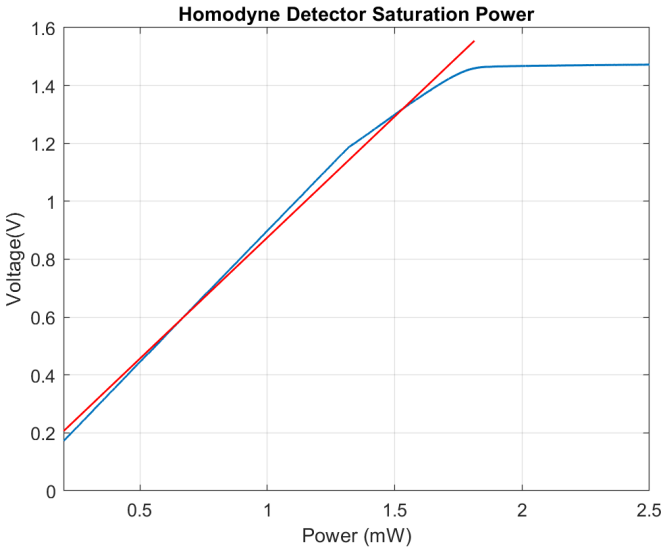

Figure 22: BHD saturation power

From the plot in figure 22 it is clear that up to the injected power value of 1.8mW the response of the detector is linear while after that threshold value the BHD saturates exhibiting a constant trend. It is therefore necessary to point out that even if this value marks a saturation in the BHD minitoring outputs, the differences in fluctuations of the two signals, probed by the spectrum analyzer, shows a significant behaviour up to the considered value of circa 3mW, after that, the BHD saturation badly affects the noise level, determining unreasonable value which shall not be taken into consideration.

3.4.2 Experimental setup for squeezing measurements

The experimental setup involved in the measurement of squeezing exploits elements from both the two previous sections, the OPA and BHD, and it is reported in figure 23.

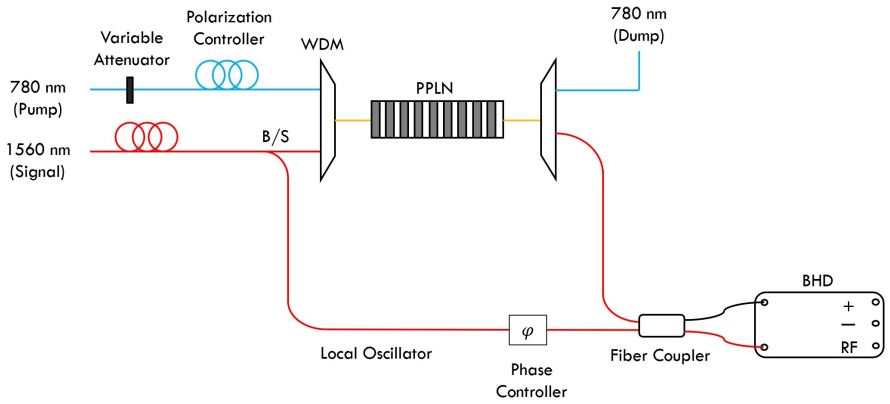

Figure 23: Squeezing measurement setup

As described in section 2.3, the key point in BHD is the presence of a Local Oscillator (LO) beam which phase is scanned, similarly to what was done in the OPA setup for the phase-dependent gain. As figure 23 shows, a fibered beam splitter serves to split the input signal beam for it to act as the LO while the squeezed light is collected by a second WDM. Both these two beams are made to interact with one another exploiting a 2-by-2 fiber coupler which outputs are fed to the BHD following a similar data acquisition as in figure 20 with the spectrum analyzer and the oscilloscope, which for the sake of simplicity have been excluded from this figure.

3.4.3 Measurements

The measurement of squeezing is a procedure which is extremely dependent on the noise of the system which is particularly detrimental to the clear observation of the squeezing sprectum itself. An example can be observed from figure 24 where the oscillations of the noise power periodically overcome the limit of shot noise, characterized as a function of the power in the previous section, certifying indeed that the light emitted from an optical parametric amplifier shows correlation between its quadratures that yields a reduction of the fluctuations of one of such quadratures able to reach below the SQL at the cost of an increase in the other quadrature[11][12].

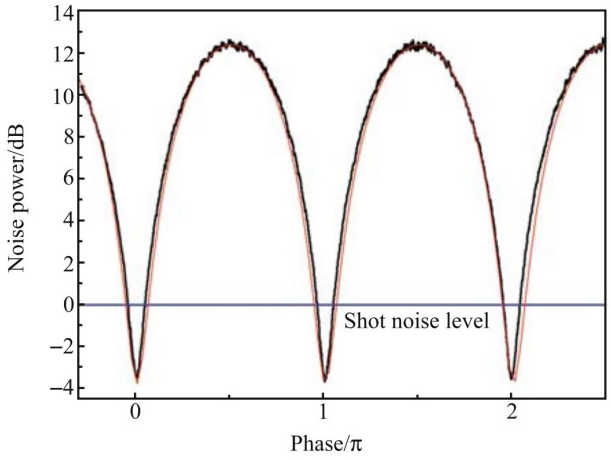

Figure 24: Squeezing measurement example

4 Conclusion and Perspectives

The perspectives in the use of $LiNbO_3$ for quantum optics are many, here are reported three main routes that may be followed to exploit the capabilities of this material in the field of quantum optics and more broadly speaking quantum communication.

4.1 Single photon level - Discrete Variable

The work presented in this report refers to a many-photons regime, also known as continous variable (CV). One of the most promising directions to follow is the use of the PPLN platform at the single-photon level, also known as discrete variable (DV). To realize photonic integrated circuits (PICs) which can be used to generate and manipulate different states of light with the implementation of more complex structures such as systems for entanglement swapping etc. [13] Such structure can be designed and implemented on a single LNOI chip, including all the elementary operations (phase shifters, beam splitters etc.) guaranteeing a better efficiency and reliability[14].

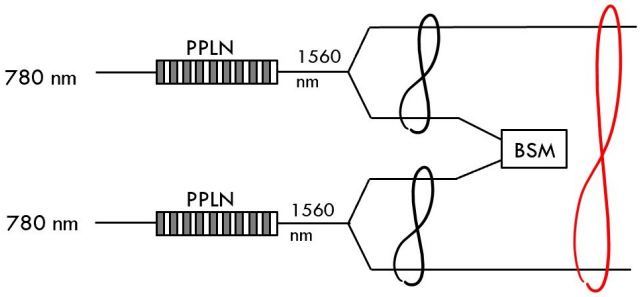

Figure 25: Entanglement Swapping

4.2 Multi-mode entanglement - Continuous Variable

The generation of squeezed states by means of PPLN in PICs can exploit the natural energy-time entanglement of the generated twin photons, by designing the circuit in a proper way it could be possible to generate light states of multiple entangled modes rather than only two, this would extend the number of degrees of freedom that can be exploited.

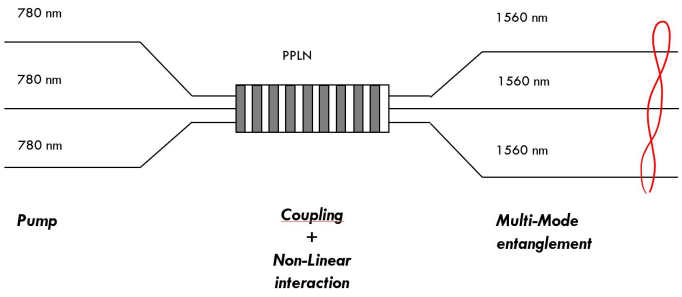

Figure 26: Multi-Mode Entanglement

4.3 Non-Gaussian states of light - Hybrid approach

Non-Gaussian states of light are light states whose fluctuations do not have a Gaussian distribution which is the case for squeezed states for example. Squeezed states themselves are, however, the starting point for the generation of Non-Gaussian states, this could be done with the removal of a single photon from a squeezed state exploiting a weak coupling regime among the three waveguides. PPLN could be, in conclusion, a promising platform for the "on-demand" generation of Non-Gaussian states of light.[6]

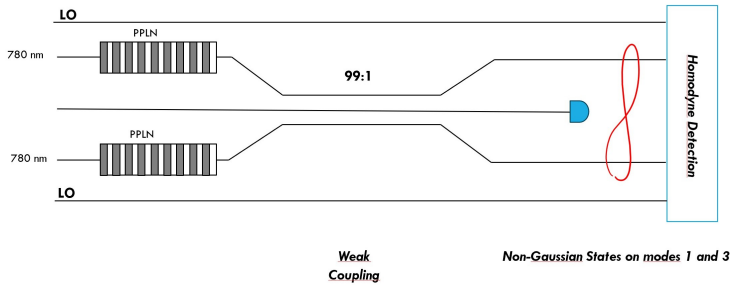

Figure 27: Non-Gaussian States Generation

References

[1] Hans-A. Bachor. *A guide to experiments in quantum optics*. Wiley-vch, 1998.

[2] Zhu et al. integrated photonics on thin film lithium niobate.

[3] A. Boes et al. "Status and potential of Lithium Niobate on Insulator (LNOI) for Photonic Integrated Circuits". In: *Laser Photonics rev.* (2018).

[4] Weidong Chen et al. "Continuous-wave mid-infrared laser sources based on differencefrequency generation". In: *C. R. Physique* (2007).

[5] Dr. Rüdiger Paschotta, RP photonics, Quasi Phase Matching.

[6] A.I. Lvovsky et al. "Production and applications of Non-Gaussian quantum states of light". In: *arXiv* (2020).

[7] R. Loudon. *The Quantum Theory of Light*. Oxford Univeristy Press, 2000.

[8] Kamel Bencheikh. "Traitement non destructif des signaux optiques". PhD thesis. Université Paris XIII, 1996.

[9] Mark Fox. *Quantum Optics, an introduction*. Oxford University Press, 2005.

[10] A. Henry et al. "Correlated twin photons generation in a silicon nitride loaded thin film PPLN waveguide". In: *Optics Express* (2023).

[11] Y. Zhang. "Generation of non-classical states from an optical parametric oscillator/amplifier and their applications." In: *Front. Phys. China* (2008).

[12] T. Park et al. "Single-mode squeezed light generation and tomography with an integrated optical parametric oscillator". In: *arXiv* (2023).

[13] Y. Li et al. "Multiuser time-energy entanglement swapping based on dense wavelength division multiplexed and sum frequency generation". In: *Physical Review Letters* (2019).

[14] J. Zhao et al. "High quality entangled photon pair generation in periodically poled lithium niobate waveguides". In: *Physical Review Letters* (2020).